Ocean Engineering 335 (2025) 121704

Contents lists available at ScienceDirect

Ocean Engineering

journal homepage: www.elsevier.com/locate/oceaneng

Research paper

CMIP6 projections of wave climate change in the Mediterranean sea by the end of the twenty-first century

Gabriel Ibarra-Berastegui [a,b,*], Jon Sáenz [b,c], Alain Ulazia [d], Santos J. González-Rojí [b,c], Ganix Esnaola [b,e]

[a] Energy Engineering Department, University of the Basque Country (UPV/EHU), Plaza Ingeniero Torres Quevedo, 1, Bilbao, 48013, Spain
[b] Plentzia Itsas Estazioa, UPV/EHU, Areatza Hiribidea, 47, Plentzia, 48620, Spain
[c] Department of Physics, University of the Basque Country (UPV/EHU), Barrio Sarriena, Leioa, 48940, Spain
[d] Energy Engineering Department, University of the Basque Country (UPV/EHU), Otaola Hiribidea, 29, Eibar, 20600, Spain
[e] Energy Engineering Department, University of the Basque Country (UPV/EHU), Plaza Europa, 1, Donostia, 20018, Spain

ARTICLE INFO

Keywords:
CMIP6 models
WaveWatch-III
Trends
Wave energy flux
Surface wind
Significant wave height
Mean wave period

ABSTRACT

Recently published wave simulations from WaveWatch-III, corresponding to eight Coupled Model Intercomparison Project Phase 6 (CMIP6) global climate models, were used to estimate the changes in the significant wave height, mean wave period, wave energy flux, and sea surface winds in the Mediterranean basin projected for 2100. The resolution of the data was $0.5° \times 0.5°$, and projections were calculated for SSP126 and SSP585 shared socioeconomic pathways. With respect to the current situation, for the Shared Socioeconomic Pathways 126 (SSP126 scenario), an almost static picture emerges, with some small areas in the East Mediterranean exhibiting minor positive trends. Under the SSP585 scenario, significant negative trends are expected throughout the Mediterranean region. Under this scenario, the 2010–2020 decade represents a tipping point in the Mediterranean, in contrast to previous decades, where almost constant values were recorded.

1. Introduction

1.1. Climate models

The last assessment report (AR6) by the Intergovernmental Panel on Climate Change (IPCC) IPCC (2022); Masson-Delmotte et al. (2021) included the results of the most recent projections derived from the CMIP6 (World Climate Research Program, 2021; Hellmuth et al., 2025) for a large number of atmospheric variables. Several scenarios have been considered depending on the future evolution of greenhouse gas (GHG) emissions (O'Neill et al., 2016). From the entire set of shared socioeconomic pathways, the so-called SSP126 (lowest emissions) and SSP585 (the most pessimistic) (Van Vuuren et al., 2011, 2014; Kriegler et al., 2014; Riahi et al., 2017) scenarios regarding future cuts in GHG emissions (DKRZ, 2022) were the most extreme cases used in AR6. The rest correspond to the socioeconomic pathways between both extremes. CMIP3 (Meehl et al., 2020) and CMIP5 (Kajtar et al., 2021) represent the two previous generations of integrations coordinated by the IPCC over the past decade.

However, a comprehensive analysis of the impact of climate variation on seas and oceans requires both an evaluation of current and past observations and the use of wave models fed with wind outputs from CMIP models to assess their future evolution.

The main variables of interest used to characterise the general physical behaviour of ocean basins are typically:

1. Significant wave height (H_s, m). Represents the average of the highest one third of the observed individual waves' heights. It is widely used in meteorology and also in navigation.
2. Mean wave period (T_m, s). At a given sea-state, it is the average period of the recorded period between each pair of subsequent waves.
3. Wave energy flux (WEF, $\mathrm{kW\,m^{-1}}$). It is the main indicator used to describe the energy held by waves and is widely used as one of the main indicators of feasibility for potential wave energy farms locations.
4. Because these oceanic variables originate from wind blowing above the sea surface, the evolution of wind speed (U, $\mathrm{m\,s^{-1}}$) should also be analysed if a complete picture of a sea basin is to be given.

After a preliminary evaluation of existing literature by basins, it was detected that the Mediterranean Sea is the area where projections of WEF, U, H_s and T_m by 2100 exhibit the most negative decreasing trends under the SSP585 scenario. Furthermore, according to some studies

* Corresponding author.
E-mail addresses: gabriel.ibarra@ehu.eus (G. Ibarra-Berastegui), jon.saenz@ehu.eus (J. Sáenz), alain.ulazia@ehu.eus (A. Ulazia), santosjose.gonzalez@ehu.eus (S.J. González-Rojí), ganix.esnaola@ehu.eus (G. Esnaola).

https://doi.org/10.1016/j.oceaneng.2025.121704
Received 8 January 2025; Received in revised form 8 May 2025; Accepted 28 May 2025
Available online 7 June 2025

collected in a recent extensive review (Lionello et al., 2023), is also one of the areas that has been warming more rapidly over the last decades.

For this reason, this study focuses on the Mediterranean Sea.

1.2. Past observations in the Mediterranean basin

Several studies have analysed the evolution of different oceanic variables in recent decades (Reguero et al., 2019; Odériz et al., 2021; Young and Ribal, 2019), revealing important differences among ocean basins.

The studies for the Mediterranean have analysed the historical trends since 1950 of H_s using different divisions by sub-basins and sub-regions (Barbariol et al., 2021; Elshinnawy and Antolínez, 2023). In some cases, negative trends of H_s have been reported (Elshinnawy and Antolínez, 2023), although a recent extensive review highlights the lack of consensus among authors (De Leo et al., 2024). However, it must be noted that based on the past evolution in the Mediterranean basin, other studies (Reguero et al., 2019; Young and Ribal, 2019; Gao et al., 2021) focusing on recent decades have described an almost static picture with minor changes in the oceanic variables analysed here.

1.3. Current projections for the Mediterranean

A review of the literature available indicates that an analysis on the future evolution of the Mediterranean should be first put in the context of the global projections for the Earth's oceans.

CMIP5-based studies (Patra et al., 2021b; Morim et al., 2020) suggest for the 2081–2099 period an important geographical asymmetry for the wave energy flux (WEF, $\mathrm{kW\,m^{-1}}$). These simulations project higher values in the Southern Hemisphere and lower values in the Northern Hemisphere compared to the current-day values. Similarly, CMIP6-derived projections of the significant wave height (H_s, m) and mean wave period (T_m, s) for the 2071–2100 period also indicate a similar asymmetry between both hemispheres (Meucci et al., 2024), with important geographical differences. Regarding U, positive trends in wind speed for most areas over the ocean have been reported for 1985–2018 (Young and Ribal, 2019). Some projections of CMIP5 (Casas-Prat et al., 2018) and CMIP6 (Meucci et al., 2024, 2023) for the last decades of the 21st century over ocean areas indicate a general reduction in the average wind speed values. Additionally, a recent extensive study by authors combining 39 CMIP6 projections until 2100 (Esnaola et al., 2024) suggested that the evolution of wind speed is not uniform throughout all basins and is highly dependent on the final scenario.

Coming to the Mediterranean, the initial studies on the future evolution of the Mediterranean, based on CMIP3 integrations, Mori et al. (2013); Semedo et al. (2012) suggested negative trends of H_s for this basin. Later publications using CMIP5 (Casas-Prat et al., 2018; Lemos et al., 2019; Lira-Loarca et al., 2021) and CMIP6 integrations for the area (Rusu, 2025) also confirmed projected declining trends of H_s in the Mediterranean Sea. Similarly, a recent study on the area (Rusu, 2024) incorporated a SWAN (Holthuijsen et al., 2023) integration fed by the CMIP6 model ALADIN (Spiridonov et al., 2023). The study suggested a slight increase in WEF for 2041–2070 under the SSP585 scenario. In the case of U, several CMIP6 projections (Esnaola et al., 2024; Martinez and Iglesias, 2021, 2023) indicate negative trends in wind speed for the Mediterranean basin under the SSP585 scenario by 2100.

1.4. Objectives

For the Mediterranean Sea, beyond the initial projections by 2100 commented above, a more comprehensive evaluation of trends corresponding to the whole set of oceanic variables is needed, both at local and basin level. To that purpose, here, the most recent CMIP6-derived projections of WEF, U, H_s and T_m from 2015 to 2100 have been used to estimate changes in these oceanic variables by the end of the 21st century. Researchers at CSIRO (Meucci et al., 2023) have obtained three-hourly global wave data by feeding wind outputs from eight CMIP6 models (World Climate Research Program, 2021) into the WaveWatch-III (WW3) wave model (Wavewatch III Development Group, 2016). As a result, wave data covering 1961–2100 are freely available to the scientific community (Meucci et al., 2021b,a) and were used in this study, focusing on the Mediterranean basin. These CMIP6-derived projections provide the highest time (3 h) and space resolution (0.5°) obtained so far. The results correspond to the two extremes (lowest and highest) shared socioeconomic pathways (SSP126 and SSP585, respectively) available from the CSIRO WaveWatch III-based wave simulations until 2100 for the Mediterranean.

Following the generally accepted criteria (World Meteorological Organization, 2017; American Meteorological Society, 2022; ECMWF, 2021), a 30-year period was selected to characterise current-day conditions. For this purpose, the averages for the 1985–2014 period of the above mentioned four variables from the fifth-generation ECMWF reanalysis, ERA5 (Hersbach et al., 2020; ECMWF, 2021), were adopted as the baseline.

Given the different time coverage of data from the eight CMIP6 models, the general objective of this study was to assess the projections of oceanic variables in the Mediterranean Sea by 2100 using two different complementary approaches. The oceanic variables analysed were WEF, U, H_s and T_m with a special focus on significant averages and robust trends. The specific objectives were as follows

1. For the eight CMIP6 models, 3-hourly WW3 integrations are available for the 1985–2014 (historical, adopted as a description of current-day conditions) and 2071–2100 periods. In this case, spatial averages for both periods were calculated and compared for the Mediterranean Sea to detect significant changes in the overall regional means.
2. Additionally, in the case of two of those models (EC-EARTH3 Döscher et al., 2021 and ACCESS-CM2 Bi et al., 2020), complete WW3 integrations of 3-hourly data running from 1985 to 2100 are also available. This has also made it possible to calculate grid point-by-grid point trends for the whole period.
3. The consistency of the joint trends of WEF, U, H_s and T_m were assessed for all the grid points covering the Mediterranean basin.
4. The trends for the 2015–2100 period were discussed for both scenarios (SSP126 and SSP585) and in the light of the past behavior of the Mediterranean Sea as reported for the previous decades before 2015.

The effects of sea level change (Lee and Romero, 2023), future projections of extremes (Vanem, 2017; Lobeto et al., 2021; Patra et al., 2021a), and uncertainties derived from climate oscillations in the return period of waves (Ewans and Jonathan, 2023) fall beyond the scope of this study. For all calculations, plots, tables, and text, authors adopted the geographical boundaries of the Mediterranean basin as officially defined by the IPCC (Iturbide et al., 2020).

The remainder of this paper is organised as follows: After this introduction, in Section 2 data used and methodology followed are explained. Results are presented in Section 3, are discussed in Section 4 and conclusions can be found in Section 5.

2. Data and methodology

This section describes the data and methodology used in the study.

2.1. Data

The Mediterranean basin data used in this study were obtained from two sources:

1. ERA5 reanalysis of hourly data with a $0.5° \times 0.5°$ resolution corresponding to the 1985–2014 period (ECMWF, 2024). The downloaded variables include the following:

a) significant height of combined swell and wind waves (H_s)
b) mean wave period (T_m)
c) zonal component of wind speed 10 m above sea level
d) meridional component of wind speed 10 m above sea level.

ERA5 did not provide a direct estimation of WEF values. Therefore, the hourly wave energy flux was calculated using the deep-water hypothesis for all the Mediterranean grid points according to the following equation (Bidlot, 2016; Multon, 2013):

$$\mathrm{WEF} = 0.49 \cdot T_m \cdot H_s^2 \tag{1}$$

2. Three-hourly zonal and meridional wind components, WEF, H_s and T_m values corresponding to the 2015–2100 projections from the CSIRO repository (Meucci et al., 2023, 2021b). These are the WW3 outputs obtained after entering the wind outputs from the two CMIP6 models (EC-EARTH3 Döscher et al., 2021 and ACCESS-CM2 Bi et al., 2020) under two scenarios (SSP126 and SSP585). In addition, the historical three-hourly values of the same models for 1985–2014 were downloaded.

Finally, WW3 outputs of the historical period (1985–2014) and the final decades of the 21st century (2071–2100) corresponding to six additional models (AWI-CM-1-1-MR, CMCC-CM2-SR5, IPSL-CM6A-LR, KIOST-ESM, MPI-ESM1-2-LR, and MRI-ESM2-0), also made available to the scientific community by CSIRO (Meucci et al., 2023, 2021b), were used in this study.

CMIP6 projections corresponding to the eight CMIP6 models were considered. These eight models cover different regions within the range of Equilibrium Climate Sensitivities in the CMIP6 ensemble (Meehl et al., 2020), ensuring that the results are not biased. However, the availability of data from different periods and the interest in a joint analysis incorporating all available models led to a dual approach (see Section 2.2) to shed light on the future evolution of oceanic variables in the Mediterranean basin by the end of the 21st century.

All variables were provided by CSIRO on the same $0.5° \times 0.5°$ grid as ERA5, thus making unnecessary a regridding stage to project data from all sources onto a common grid. A summary of the variables, periods and models can be seen in Table 1.

Table 1
ERA5 and CMIP6 models' time resolution and periods used for the four variables of this study (WEF, U, H_s, and T_m). Mediterranean basin. Space resolution is $0.5° \times 0.5°$.

	SSP126	SSP585	Historical
ERA5 (ECMWF 1h)			1985–2014
EC-EARTH3 (CMIP6-WW3 3h)	2015–2100	2015–2100	1985–2014
ACCESS-CM (CMIP6-WW3 3h)	2015–2100	2015–2100	1985–2014
AWI-CM-1-1-MR (CMIP6-WW3 3h)	2071–2100	2071–2100	1985–2014
CMCC-CM2-SR5 (CMIP6-WW3 3h)	2071–2100	2071–2100	1985–2014
IPSL-CM6A-LR (CMIP6-WW3 3h)	2071–2100	2071–2100	1985–2014
KIOST-ESM (CMIP6-WW3 3h)	2071–2100	2071–2100	1985–2014
MPI-ESM1-2-LR (CMIP6-WW3 3h)	2071–2100	2071–2100	1985–2014
MRI-ESM2-0 (CMIP6-WW3 3h)	2071–2100	2071–2100	1985–2014

2.2. Methodology

The methodology used in this study consisted of six major steps.

1. **Characterisation of current-day values of** WEF, U, H_s **and** T_m. Starting with ERA5 hourly records at each grid point of the $0.5° \times 0.5°$ grid, time averages corresponding to the 1985–2014 period were computed.

As mentioned earlier, this period was adopted as the reference period for characterising the current-day situation and evaluating future departures. These averages were calculated both as yearly averages (YE) (Fig. 1) and also by seasons of the year (Appendix A, Figs. A1, A2, A3, and A4). For this purpose, the year was divided into the four seasons for the Northern Hemisphere (Reguero et al., 2015; Camus et al., 2019): summer (SU) running from June to August; autumn (AU) from September to November; winter (WI) from December to February; and spring (SP), from March to May.

2. **Calculation of monthly anomalies.** For the four variables analysed, eight models, and two scenarios, monthly averages were computed for the 1985–2100 period. Then, using only the 1985–2014 period for the CMIP6 models (historical) as a reference, monthly averages were calculated to characterise the seasonal cycle at each ocean grid point. Finally, monthly anomalies of WEF, U, H_s and T_m were computed by subtracting the seasonal cycles obtained from the monthly averages derived from the WW3 outputs.

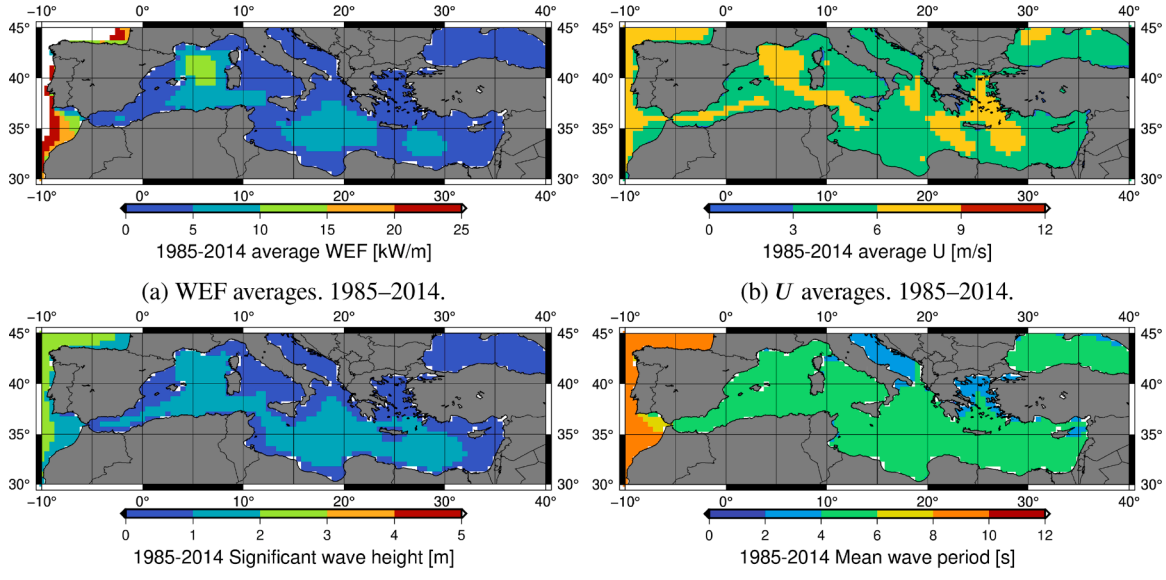

(a) WEF averages. 1985–2014. (b) U averages. 1985–2014.

(c) H_s averages. 1985–2014. (d) T_m averages. 1985–2014.

Fig. 1. ERA5 baseline averages for the Mediterranean basin. Period: 1985–2014.

3. **Comparison of aggregated regional averages between 1985–2014 and 2071–2100.** Since the evolution of geophysical fields is not expected to follow a linear evolution under the different shared socioeconomic pathways, it is often considered that the evolution of spatial monthly or yearly averages of the different geophysical fields is indicative of the time evolution. For instance, refer to the Sixth Assessment Report of the IPCC (Masson-Delmotte et al., 2021). In this study, since the gridded data span different latitudes, it must be considered that the spatial average cannot consist of a direct average of the elements in the grid. This weighting by the latitude of every grid point is typical when working with regular longitude/latitude grids, whether for averaging (Gleisner, 2011) or for EOF calculation (North et al., 1982). For every grid cell centred in the longitude λ_c and latitude θ_c of a regular latitude-longitude grid with resolution given by $\Delta\lambda$ and $\Delta\theta$, the area corresponding to every grid cell can be expressed as a function of the latitude of the central point in the grid element θ_c using the equation

$$S(\theta_c) = R_e^2 \Delta\lambda \sin\left(\frac{\Delta\theta}{2}\right) \cos\theta_c. \quad (2)$$

Therefore, when calculating spatial averages, such as in Fig. 2, the spatial value of the field is first calculated by determining the weighted average that considers the different sizes of every grid cell. Then, the confidence intervals (C.I.) of the trends or the changes in the mean are calculated to obtain spatial averages by bootstrap resampling with 1000 resamples in all cases.

4. **Calculation of robust trends (2015–2100) relative to 1985–2014 historical ERA5 values.** Using monthly anomalies for the 2015–2100 period, robust Theil-Sen trends (Theil, 1950; Kumar, 1968) were calculated at each grid point for the four variables analysed, along with two models and scenarios. The Theil-Sen approach involves the calculation of multiple trends computed on

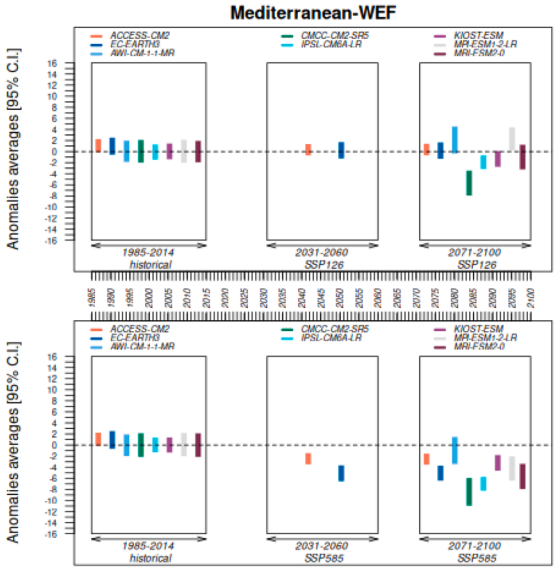

(a) WEF projections. SSP126 and SSP585 scenarios.

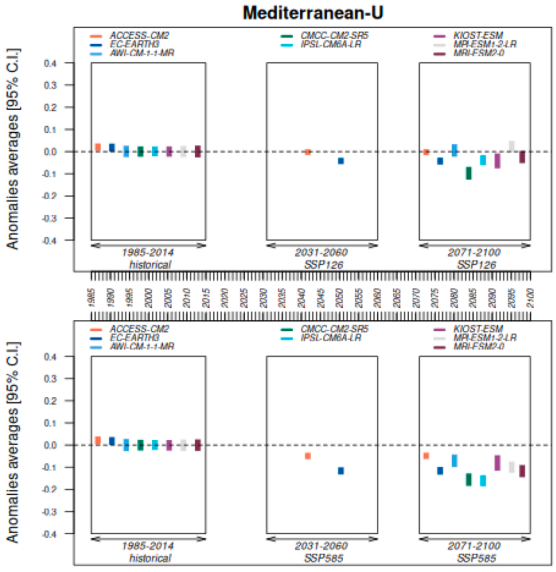

(b) U projections. SSP126 and SSP585 scenarios.

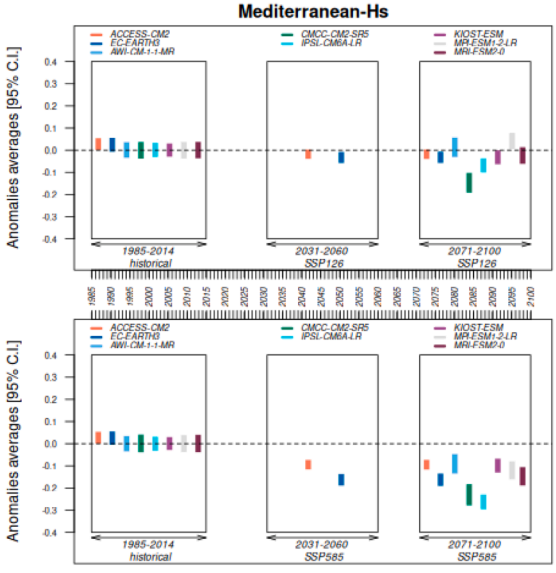

(c) H_s projections. SSP126 and SSP585 scenarios.

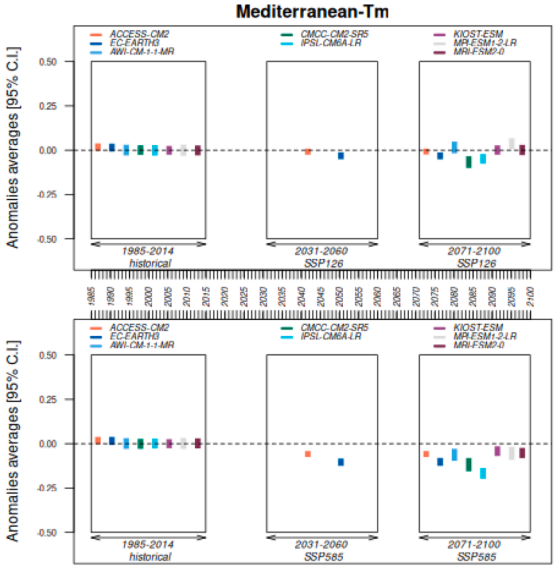

(d) T_m projections. SSP126 and SSP585 scenarios.

Fig. 2. Mediterranean Sea. CMIP6 averages (95 % C.I., calculated by bootstrap resampling with 1000 resamples). SSP126 and SSP585 scenarios obtained from monthly anomalies. Historical (1985–2014), 2031–2060 and 2071–2100 periods.

Table 2
Average trends (EC-EARTH3 and ACCESS-CM2) for both scenarios in the Mediterranean basin for the 2015–2100 period in percentage terms per decade relative to the 1985–2014 reference period. The average trends are calculated only on grid points (GP) with a significant trend. Percentage of oceanic grid points without significant trends (No_trend), positive trends (Pos_trend), and negative trends (Neg_trend) are also provided.

		SSP126				SSP585			
	Variable	Trend [%/dec]	No_trend [%]GP	Pos_trend [%]GP	Neg_trend [%]GP	Trend [%/dec]	No_trend [%]GP	Pos_trend [%]GP	Neg_trend [%]GP
Yearly	WEF	−0.45	90.96	1.09	7.95	−1.21	7.70	0.00	92.30
	U	−0.52	98.58	0.08	1.34	−0.89	22.43	0.00	77.57
	H_s	−0.83	99.33	0.00	0.67	−1.70	25.52	0.00	74.48
	T_m	−0.14	99.41	0.08	0.50	−0.58	29.87	0.00	70.13
Summer (SU)	WEF	−0.39	98.83	0.08	1.09	−1.85	17.24	0.00	82.76
	U	0.06	93.56	3.93	2.51	−0.55	31.38	3.68	64.94
	H_s	0.37	98.83	1.00	0.17	−1.18	24.77	0.25	74.98
	T_m	0.01	97.41	1.17	1.42	−0.38	21.17	0.17	78.66
Autumn (AU)	WEF	−1.77	69.21	0.00	30.79	−2.66	15.90	0.00	84.10
	U	−0.50	60.84	0.17	39.00	−0.76	10.79	0.00	89.21
	H_s	−0.98	57.82	0.00	42.18	−1.50	8.20	0.00	91.80
	T_m	−0.30	61.26	0.00	38.74	−0.53	8.03	0.00	91.97
Winter (WI)	WEF	−1.01	99.16	0.08	0.75	−1.94	50.79	0.00	49.21
	U	−0.08	88.20	4.27	7.53	−0.62	9.04	0.00	90.96
	H_s	−0.18	86.95	3.26	9.79	−1.12	9.71	0.00	90.29
	T_m	−0.06	86.11	3.01	10.88	−0.42	5.52	0.00	94.48
Spring (SP)	WEF	1.48	94.39	5.61	0.00	−2.52	51.80	0.00	48.20
	U	0.26	88.54	11.21	0.25	−0.71	50.71	0.42	48.87
	H_s	0.56	95.15	4.85	0.00	−1.21	37.74	0.25	62.01
	T_m	0.21	93.47	6.44	0.08	−0.43	26.61	0.17	73.22

every possible couple of cases on the database. The median of this statistical distribution of trends is taken as the actual trend, and its significance is estimated based on the 95 % boundaries of the group of trends calculated.

Here, only statistically significant Theil-Sen trends at a 95 % confidence level were considered. Then, at each grid point, the average trends for each scenario were calculated since both models (EC-EARTH3 and ACCESS-CM2) were considered equally reliable. The values of these trends for both scenarios (SSP126 and SSP585) and the four variables (WEF, U, H_s and T_m) at each ocean grid point were computed and expressed in percentage terms per decade relative to current-day (1985–2014) ERA5 baseline values. The mean wave period adopted in this study (T_m) corresponds to that used in the ERA5 wave model, denominated as the energy period (Bidlot, 2016). This energy period was used to calculate ERA5 WEF values Eq. (1).

However, the mean wave period output obtained from WW3 (T_{m02}) is calculated differently (Wavewatch III Development Group, 2016). To provide trend values of T_m in percentage terms, this difference was corrected at each grid point by comparing ERA5 and average models' outputs during the common historical period (1985–2014). This typically yielded a factor between 0.9 and 0.7 with small variations around these values, showing a general agreement with the ratios published by other authors (Cahill and Lewis, 2014; Gao et al., 2021). This grid point-by-grid point correction of T_{m02} allowed for the calculation of T_m trends in percentage terms relative to current-day ERA5 T_m averages.

As a result, for each grid point, projected trends of WEF, U, H_s and T_m were calculated for the 2015–2100 period, considering two models and two scenarios (SSP126 and SSP585).

5. **Calculation of latitude-corrected trends for the Mediterranean grid points.** To provide a more aggregated view of the Mediterranean, average values of trends from the two models were combined and computed for both scenarios. Additionally, the proportions of grid points with no trend, positive trends, and negative trends were also calculated for the Mediterranean basin.

To calculate these geographically aggregated trends, surface-weighted averages were used to account for the differences in the areas, depending on the latitude for the regular longitude-latitude $0.5° \times 0.5°$ grid, as mentioned above.

The results (see Section 3) of the trends for the two scenarios are presented in Table 2, Fig. 3, and Appendices B and C.

6. **Assessment of the relative influence of H_s and T_m trends on the observed** WEF **trends**. Starting from Eq. (1), it is possible to assess the evolution of WEF during the projected decades and obtain a mathematical expression of how it relates to the evolution of H_s and T_m. Thus, the derivatives of Eq. (1) with time can be used to relate WEF trends with H_s and T_m changes:

$$\frac{d\mathrm{WEF}}{dt} = 2 \cdot 0.49 \cdot T_m \cdot H_s \cdot \frac{dH_s}{dt} + 0.49 \cdot H_s^2 \cdot \frac{dT_m}{dt} \tag{3}$$

By multiplying and dividing by H_s and T_m, the two elements of the right side, the following Eq. (4) is obtained:

$$\frac{d\mathrm{WEF}}{dt} = 2 \cdot \mathrm{WEF} \cdot \frac{dH_s}{H_s \cdot dt} + \mathrm{WEF} \cdot \frac{dT_m}{T_m \cdot dt} \tag{4}$$

Finally, by dividing both sides by WEF, the following Eq. (5) is obtained, expressed as a relationship between differentials:

$$\frac{d\mathrm{WEF}}{\mathrm{WEF} \cdot dt} = 2 \cdot \frac{dH_s}{H_s \cdot dt} + \cdot \frac{dT_m}{T_m \cdot dt} \tag{5}$$

This equation indicates that the impact of H_s changes on the long-term trends of WEF is twice as significant as that of T_m. Eq. (5) has also been used to provide a general idea of consistency in the results, if as in this case, the trends are shown as [%] per decade for the three variables.

3. Results

After calculating the anomalies of WEF, U, H_s and T_m for the eight models and two scenarios (SSP126 and SSP585), the temporal and spatial averages for the Mediterranean basin were computed for the three periods: 1985–2014 (historical or baseline), 2031–2060 (mid-century), and 2071–2100 (end of the century). In Fig. 2, each colour bar represents the 95 % confidence boundaries of the aggregated spatial averages for each model and period. As mentioned above, for the 2031–2060 period, only data corresponding to the EC-EARTH3 and ACCESS-CM2 integrations were available.

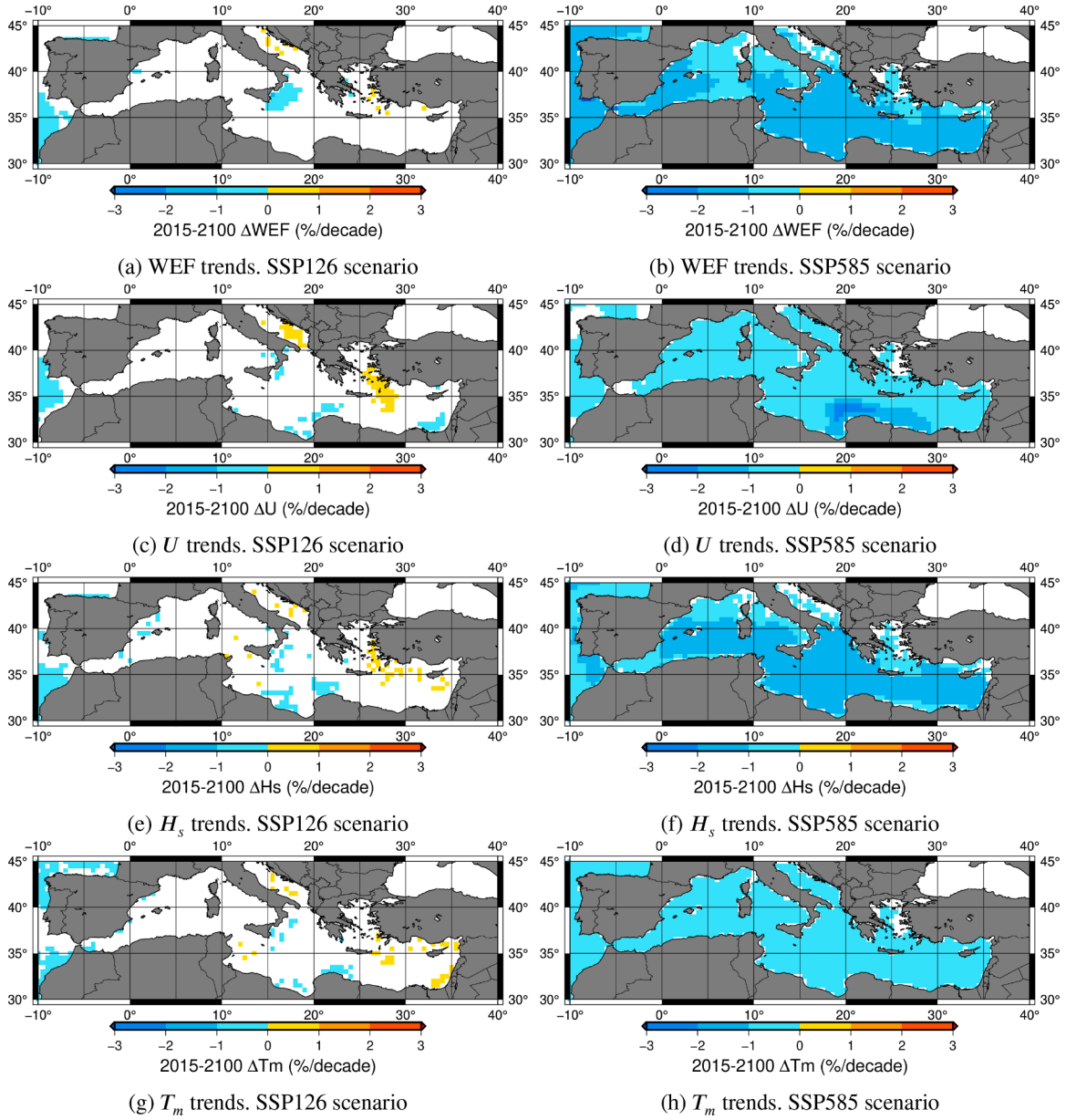

Fig. 3. CMIP6-derived 2015–2100 trends [%/decade] with respect to the 1985–2014 period. SSP126 and SSP585 scenarios.

Fig. 2 shows the information corresponding to each of the three periods for the two scenarios, making it possible to detect the overall changes in the Mediterranean basin. The overlapping colour bars corresponding to two different periods indicated non-significant changes, whereas disjoint colour segments indicated significant changes at the 95 % confidence level. After calculating the Theil-sen trends at each grid point, the latitude-corrected average trends for the Mediterranean were determined and are presented in Table 2, while Fig. 3 shows their spatial distribution. These results are analysed for the two scenarios considered.

1. **Changes until 2071–2100 under the SSP126 scenario.**

   For the SSP126 scenario, out of the eight models, seven indicated no significant changes in the aggregated averages of WEF, U, H_s and T_m throughout the Mediterranean at a 95 % confidence level. The only model with non-overlapping 95 % confidence bars between 1985–2014 and 2071–2100 was the CMCC-CM2-SR5. Therefore, this analysis suggested decreasing values of WEF, U, H_s and T_m by the end of the 21st century for the Mediterranean basin.

   Under this scenario, the projections of the EC-EARTH3 and ACCESS-CM2 models for the 2031–2060 period also indicated no significant changes in the averages for the Mediterranean Sea. These results strongly implied an overall static picture for the Mediterranean basin taken as a whole during the 21st century relative to the historical or baseline period (1985–2014) for the SSP126 scenario. Table 2 confirmed the results with a percentage ranging from 90 % (WEF) to 99 % (T_m) of grid points with no significant trend in the Mediterranean Sea area. In Fig. 3, it can be observed that under the SSP126 scenario, a small number of grid points in the Aegean and Adriatic seas and East Mediterranean area exhibited small positive individual trends, all well below 1 % per decade. Similarly, in the Central and Southern Mediterranean, some small areas showed negative trends. As a result, average trends computed only on significant trends (either positive or negative) adopt a value around 1 % for WEF and much smaller values for the rest (U, H_s, and T_m). Since WEF, H_s, and T_m were mainly driven by surface winds, U trends exhibited both a general and spatial coherence with the oceanic variable trends. It must be highlighted that when this analysis is carried out by season, the observed trends were concentrated in Autumnn (Fig. 3 (Appendix B, Figs. B1, B2, B3, and B4)). For the SSP126 scenario, all the results above provided

a consistent projection, showing no changes until the end of the century.

2. **Changes until 2071–2100 under the SSP585 scenario.**

Under the SSP585 scenario, in the case of WEF, seven models indicated lower regional averages for the final part of the 21st century (Fig. 2). The only model that suggested no changes was the AWI-CM-1-1-MR. For the remaining variables analysed (U, H_s, and T_m), all the models indicated regional lower averages by the end of the century. The 2031–2060 period averages (only EC-EARTH3 and ACCESS-CM2 integrations) also indicated declining averages for this intermediate period. Decadal trends until 2100, relative to 1985–2014 period, for the SSP585 scenario are shown in Fig. 3. Appendix C shows the trends by season. Table 2 shows that at the 95 % confidence level in the case of WEF, negative trends were projected at most grid points for all four variables analysed. The most negative values [% /decade] were concentrated in the variables WEF and T_m, particularly in autumn and summer. Thus, under this scenario, the above results were consistent with a significant reduction of U, WEF, H_s, and T_m by 2100.

Compared to the current-day ERA5 observations, in which all variables exhibited important differences throughout the Mediterranean Sea (Fig. 1), the projected trends showed a far more homogeneous spatial distribution, although they tended to concentrate in the Southern part of the Mediterranean.

4. Discussion

At a global level, several studies have analysed the evolution of wave energy fluxes (WEF, $\mathrm{kW\,m^{-1}}$) and ocean surface winds (U, $\mathrm{m\,s^{-1}}$) during the last few decades (Reguero et al., 2019; Odériz et al., 2021; Young and Ribal, 2019; Reguero et al., 2015; Erikson et al., 2022). All studies agreed that until the first decades of the 21st century, increases in WEF, U, and H_s (Liu et al., 2023) have been observed, showing important differences among regions. In the Southern Hemisphere, most areas exhibited a growing trend until 2010 (Reguero et al., 2015); however, in the Northern Hemisphere, some areas exhibited positive trends in WEF (Penalba et al., 2020), H_s, and T_m (Ulazia et al., 2017). A more specific analysis (Reguero et al., 2019) detected a positive trend in WEF, concluding that since 1948, a global average increase of 4.8 % per decade occurred in the ocean until 2008. Regarding U, positive trends in wind speed for most areas over the oceans have been reported for 1985–2018 (Young and Ribal, 2019). In the case of the mean wave period, authors have also reported a global increase in T_m during the 20th century (Ulazia et al., 2023), although some studies have suggested important regional differences (Gao et al., 2021) with the highest values recorded in the Southern Hemisphere. However, future projections suggest for the 2081–2099 period (Patra et al., 2021b; Meucci et al., 2024; Casas-Prat et al., 2018; Meucci et al., 2023; Erikson et al., 2022; Odériz et al., 2022; Pourali et al., 2023) suggested an substantial geographical asymmetry in WEF values. For the Southern Hemisphere, higher values of WEF and H_s (Lobeto et al., 2021) than current-day observations were predicted, whereas lower values were expected for the Northern Hemisphere.

In this general scheme, the Mediterranean basin appeared to follow a distinctive pattern, which, as discussed in Section 1, was characterised by a static pattern over the last few decades. However, under the SSP585 scenario, it shared major declining trends with the rest of the Northern Hemisphere until the end of the 21th century. Under the SSP126 scenario, an almost static picture emerged for the 2015–2100 period, with non-significant trends for most Mediterranean grid points.

The resolution of this study is for the four variables analyzed of $0.5° \times 0.5°$. Increasing the resolution of these results would perhaps provide a better assessment in some particular geographical areas, but it would involve a huge computational effort since ERA5 and the 8 CMIP6 models' integrations -both already projected onto the same geographical grid- would not be readily available as now. At a further step, we would still have to replicate all the study as shown in here.

However, it must also be noted that specially under the SSP585 scenario, a rather uniform picture emerges throughout different regions of the Mediterranean and therefore, it is reasonable to expect that with a higher resolution, the results would to a certain extent at least, reproduce the general patterns observed. Along these lines, this study represents a compromise between data availability, resolution and a realistic estimation of computational capacities.

The mechanisms driving the trends observed in this study require further investigation. Some studies suggest that the observed trends of H_s in the Mediterranean basin may be driven by the evolution of the Scandinavian index (Barbariol et al., 2021; Elshinnawy and Antolínez, 2023) At the regional level (Penalba et al., 2020; Saenz-Aguirre et al., 2022a) and in other studies with a more global focus (Reguero et al., 2015; Odériz et al., 2022), the authors found a relationship between several atmospheric patterns (including El Niño Liu et al., 2023; Odériz et al., 2020; Ramos et al., 2021) and WEF. However, global warming appeared to affect the Southern Annual Mode (SAM) and meridional surface temperature gradient (MTG), which could explain the projected differences between the two hemispheres (Patra et al., 2021b). While these findings explain the general evolution of the Northern Hemisphere and could be applied to the Mediterranean, more specific research is needed for the Mediterranean basin and the whole set of variables incorporated into this work.

Ocean wind waves are surface gravity waves generated by the action of the wind. The significant wave height (H_s) is proportional to the square of the 10-meter surface wind speed (U). In this analysis, both (H_s) and the mean wave period (T_m) reflect a combination of locally generated wind waves and swell, waves that propagated from distant storms. Swell typically consists of longer-period waves (> 8 s). The average (T_m) across the entire Mediterranean basin is around 6 seconds, indicating that the sea state is predominantly locally generated wind waves, as expected in a small, semi-enclosed basin and already pointed out by other authors (Barbariol et al., 2021). This also explains the strong spatial correlation observed between (U) and H_s climate patterns (Fig. 1).

In a relatively small and enclosed sea like the Mediterranean Sea, the driving mechanisms behind the evolution of oceanic variables analysed tend to equalise and make the spatial distribution of changes more uniform, as seen in this study. This also applied to the much smaller Black Sea where non-significant changes are projected. The most important changes are projected to occur in autumn, with the highest number of grid points simultaneously exhibiting significant trends in of WEF, U, H_s and T_m (Fig. C4).

Because all trends were given in [%/decade], Eq. (5) can be used to test the joint consistency of the WEF, *Tm*, and H_s trends throughout the Mediterranean region. At this point, it must be noted that WW3 calculates WEF from the wave spectrum. In contrast, ERA5-derived WEF values have been calculated using Eq. (1) after correcting for the wave period. It also must be noted that Theil-Sen trends are calculated from medians (not averages) and have been obtained by combining two different WW3 integrations (EC-EARTH3 and ACCESS-CM2) as well as ERA5 data. The agreement between the two sides of the equation yielded a correlation coefficient of 0.78. Despite the differences between the two sides of the equation, the correlation coefficient obtained provides reasonable confirmation of the joint consistency of the trends calculated for WEF, *Tm*, and H_s, with changes in H_s being twice as influential on WEF trends as *Tm*.

Nevertheless, in the context of global warming, a more comprehensive analysis that combines the elements known to be involved in the evolution of oceanic variables is required to explain future projections presented in this study. An analysis of trend evolution by season under the SSP585 scenario showed significant departures from the average, mainly in autumn. This may indicate a higher frequency of low-energy events and a lower occurrence of extremes. However, it should be noted

that the future evolution of extremes (Lobeto et al., 2021) requires a specific analysis that falls beyond the scope of this study.

The implications of the results of this study should be evaluated from several perspectives. One is the impact on the future development of the offshore renewable energy industry (wind and waves). Recently, extensive research outputs (Ibarra-Berastegui et al., 2023) on offshore candidate areas worldwide have been published by authors. For this purpose, the CMIP6-derived long-term trends of offshore energy production were computed. The results suggested that under the SSP126 scenario, almost no changes could be expected, whereas for the SSP585 scenario, significant changes in electricity production were projected in only a small proportion (15 %) of the existing or candidate areas. It can be concluded that the effects of global warming on the oceans are unlikely to compromise future development of offshore renewable energy facilities, which are expected to play a major role in reducing CO_2 emissions. However, future studies on extremes could help identify ocean regions that, with current technological development, may experience severe episodes, making certain locations practically unavailable.

Another issue is the evolution of the typical lifespan of a WEC or offshore wind turbine due to fatigue related to extreme events. This is an important issue considering the life-cycle assessment of marine renewable technologies. Recent studies have shown that historical projections over the last few decades have significantly worsened the structural damage caused by fatigue loads (Saenz-Aguirre et al., 2022b; Ulazia et al., 2024). Nevertheless, to the best of authors' knowledge, no specific studies have been conducted for the Mediterranean.

The historical trend of wind-wave energy hybridisation has also changed significantly in recent decades, and the co-location feasibility of wave energy converters and offshore wind turbines may be impacted in the future (Ulazia et al., 2023a). In light of previous work by the authors (Ulazia et al., 2023), it should be highlighted that future variations in wave periods at given locations can have more significant impact on the efficiency of wave energy converters (WEC) than wave height variations, due to displacement of the operational resonance point. However, long-term impacts of oceanic variables on future generation of a certain WEC depend heavily on the technology employed.

For this reason, the future techno-economic evolution of facilities that are already successfully operational requires specific studies, such as those carried out by Mutriku (Carreno-Madinabeitia et al., 2024), the only wave farm in the world currently supplying electricity for over ten years. However, in the Mediterranean, after a six-year test period in Gibraltar, the first fully operational wave farm in the Middle East (Jaffa, Israel) has recently come into operation and begun to supply electricity to the grid (Power, 2024). Its technology differs from that of Mutriku, as it relies on the motion of a set of pistons driven by the wave height. Although further research is needed, a declining trend of H_s as shown in this study under the SSP585 scenario represents a major technological challenge in the long term for the Jaffa wave farm, which may require a redesign of its operational working point.

Another important aspect is how these changes may affect navigation. The most relevant variable is the significant wave height (Kim et al., 2023). H_s exhibited negative trends in the Mediterranean Sea with a reduction of more than 1 % per decade under the SSP585 scenario. Seasonal analysis of these trends (Appendix C and Figs. C1, C2, C3, and C4) indicated an important global reduction in H_s during winter and autumn, mainly in the central area of the Mediterranean basin. The projected changes in ocean currents in the Mediterranean Sea remain unexplored, which could also affect navigation. In this sense, important benefits and cost reductions can be expected from more fluid navigation owing to the lower values of H_s in the Mediterranean. Because of its connection with the Suez Canal, the Mediterranean route is an essential element in global maritime traffic, and reductions in wave heights can reduce costs and travel times. However, it can also lead to illegal activities involving navigation, such as arms, drugs, and human trafficking, thus posing an additional security challenge for authorities. The maps show that under the SSP585 scenario, H_s reductions are expected to be more intense in the Central Mediterranean and autumn, which could redefine the preferential navigation routes and schedules for both legal and illegal activities.

5. Conclusions and future outlook

The combination of data from various sources, starting from the 20th century and future projections until 2100, was addressed collectively. A threefold approach was then used to characterise the future projections of oceanic variables:

i) Aggregated averages to compare the historical period (1985–2014) and the end of the century (2071–2100)
ii) Grid point-by-grid point robust trends from 2015 to 2100
iii) Latitude-corrected spatially-averaged trends for the whole Mediterranean Sea

This combined approach makes the conclusions obtained here robust and can be summarized as follows:

1. For the Mediterranean basin, this is the first comprehensive study using a complete set of 8 CMIP6 models providing projections until 2100 in terms of both, decadal trends and/or changes in significant time slices for the 21st century. Eq. (5) provides a confirmation of consistency for the results obtained and indicates that trends in H_s are twice as important as T_m at explaining the WEF trends.
2. These projections have been obtained for the two most representative scenarios: SSP126 and SSP585
3. The variables selected for this study are WEF, U, H_s and T_m so that a full picture for the future evolution of the oceanic behaviour in the Mediterranean can be confidently provided
4. These future trends have been obtained for both an average representative assessment of the Mediterranean and also throughout the basin with a resolution of $0.5° \times 0.5°$.
5. The results indicate that under the SSP126 scenario a static picture emerges without significant changes until 2100
6. However, under the SSP585 scenario, a declining trend for the Mediterranean basin can be devised for the 2015–2100 period.
7. Previous studies by many authors for the last decades indicate that until the 2010 decade, WEF, U, H_s and T_m have remained constant in general terms.
8. For this reason, under the SSP585 scenario, the 2010 decade represents a tipping point in which, coming from decades with constant or static values of WEF, U, H_s and T_m, negative trends are projected until 2100 starting from 2015.
9. In general terms, reductions in H_s will make navigation easier and in this context, preferential maritime routes, both for legal and illegal activities may change

Since a trend-based approach covering the period 2015–2100 was used in this study, it was also possible that oscillations around the trends obtained may also occur in the intermediate decades, but these were not captured. The first approach was carried out using 2031–2060 averages with only two models; however, a more in-depth analysis is required to characterise the evolution decade by decade. The use of loess, another regression technique used in climate studies (Clarke and Richardson, 2021), may increase the temporal resolution of future WW3 projections and provide a more detailed picture of their evolution over the next few decades. The results of this study for the variables analysed also suggested a tipping point around the 2010–2020 decade, connecting a previous period (1985–2014) with a static picture and declining trends until 2100.

Another aspect to be considered is that the current generation of models in CMIP6 does not directly provide the outputs of oceanic variables, such as those used in this study: WEF, U, H_s and T_m. Consequently, the wind output of CMIP6 needs to be fed into the wave model. The

conclusions obtained herein were based on the largest set of available, homogeneously run wave models (Meucci et al., 2024). However, as more researchers using different wave models make their ocean integrations available (Jiang et al., 2023), these projections will need to be incorporated into the analysis after a detailed comparison and bias correction phase to homogenise the results by basin. Another challenge that deserves attention is the geographical evolution of extremes and their impacts on coastal and offshore facilities.

Currently, we are working along these lines to provide a more accurate and broader understanding of the evolution of oceanic variables and their implications for the Mediterranean (Table 3).

List of abbreviations

Table 3
List of abbreviations.

Acronym	
AR6	Sixth Assessment Report
C.I.	Confidence intervals. In all cases in this paper, at a 95 % confidence level
CMIP3	Coupled Model Intercomparison Project Phase 4 (AR4)
CMIP5	Coupled Model Intercomparison Project Phase 5
CMIP6	Coupled Model Intercomparison Project Phase 6
CSIRO	Commonwealth Scientific and Industrial Research Organisation
ECMWF	European Centre for Medium-Range Weather Forecasts
ERA5	Latest reanalysis by the ECMWF
GHG	Greenhouse gases
IPCC	Intergovernmental Panel on Climate Change
T_m	Mean wave period (s)
SSP126	Shared Socioeconomic Pathway #1 with a 2100 forcing level of 2.6 W/m2
SSP585	Shared Socioeconomic Pathway #5 with a 2100 forcing level of 8.5 W/m2
H_s	Significant height of combined wind waves and swell (m)
T_m	Energy mean wave period used by ERA5 and also adopted for this study (s)
T_{m02}	Second-order mean wave period used by WW3 (s)
WEC	Wave energy converter
WEF	Wave Energy Flux ($kW\,m^{-1}$)
WW3	WaveWatch III Model
U	Wind speed 10 m above sea level ($m\,s^{-1}$)

CRediT authorship contribution statement

Gabriel Ibarra-Berastegui: Writing – review & editing, Writing – original draft, Formal analysis, Data curation, Conceptualization; **Jon Sáenz:** Methodology, Investigation, Funding acquisition; **Alain Ulazia:** Validation, Supervision, Software, Resources, Methodology; **Santos J. González-Rojí:** Writing – review & editing, Writing – original draft, Validation, Supervision, Software ; **Ganix Esnaola:** Visualization, Software, Resources, Project administration.

Declaration of competing interest

The authors declare that they have no known competing financial interests or personal relationships that could have appeared to influence the work reported in this paper.

Acknowledgements

This study was part of the project PID2020-116153RB-I00 funded by the Spanish Ministry of Science and Innovation/National Research Agency MCIN/AEI/ 10.13039/501100011033. Financial support from TED2021-132109B- C21 (HOBE) MCIN/AEI/10.13039/501100011033 and the European Union Next Generation EU/PRTR is also acknowledged. The authors also acknowledge the funding from SENyRAD (IT1694-22), which is a research group at the Basque University System of the Basque Government. All authors contributed equally to this study. The datasets used in this study are freely available from ECMWF (2024) (ERA5), the CSIRO Data Access Portal Phase 1 repository (Meucci et al., 2021b), and Climate Projections (Combined) (Meucci et al., 2021a). By combining these datasets, the 2015–2100 Theil-Sen trends of WEF, U, H_s and T_m for the Mediterranean were calculated, which can be downloaded from https://doi.org/10.5281/zenodo.14555724.

All calculations were performed within the framework of R (R Core Team, 2023; Komsta, 2019). Maps were created using Generic Mapping Tools (GMT) (Wessel et al., 2019).

Appendix A. Seasonal results

A. ERA5 1985–2100 seasonal averages for the four variables analysed: WEF, U, H_s, and T_m.

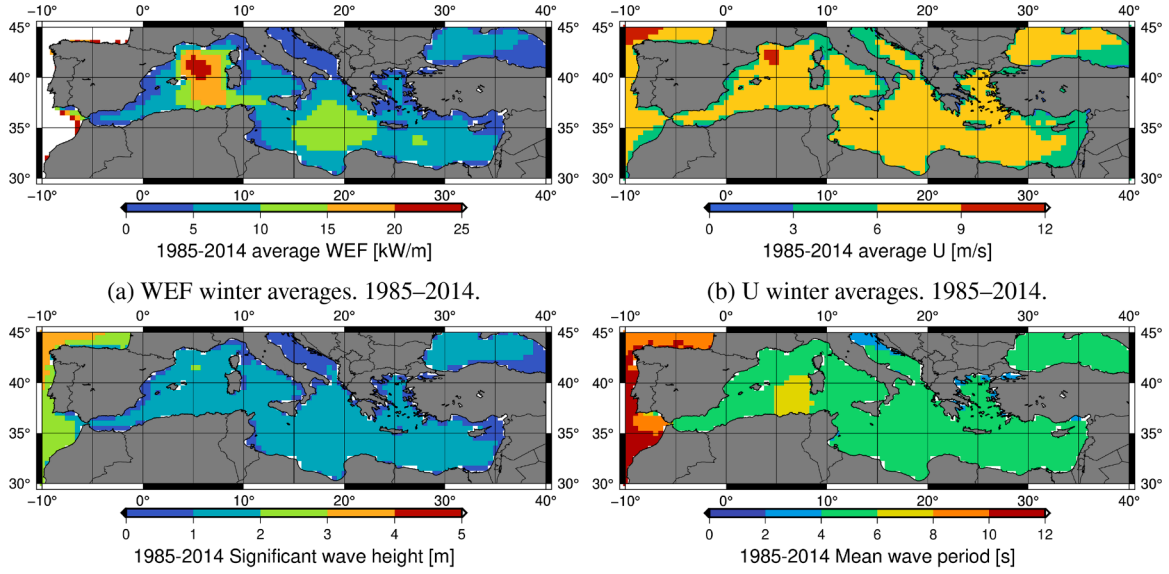

(a) WEF winter averages. 1985–2014.

(b) U winter averages. 1985–2014.

(c) H_s winter averages. 1985–2014.

(d) T_m winter averages. 1985–2014.

Fig. A1. ERA5 winter averages. 1985–2014.

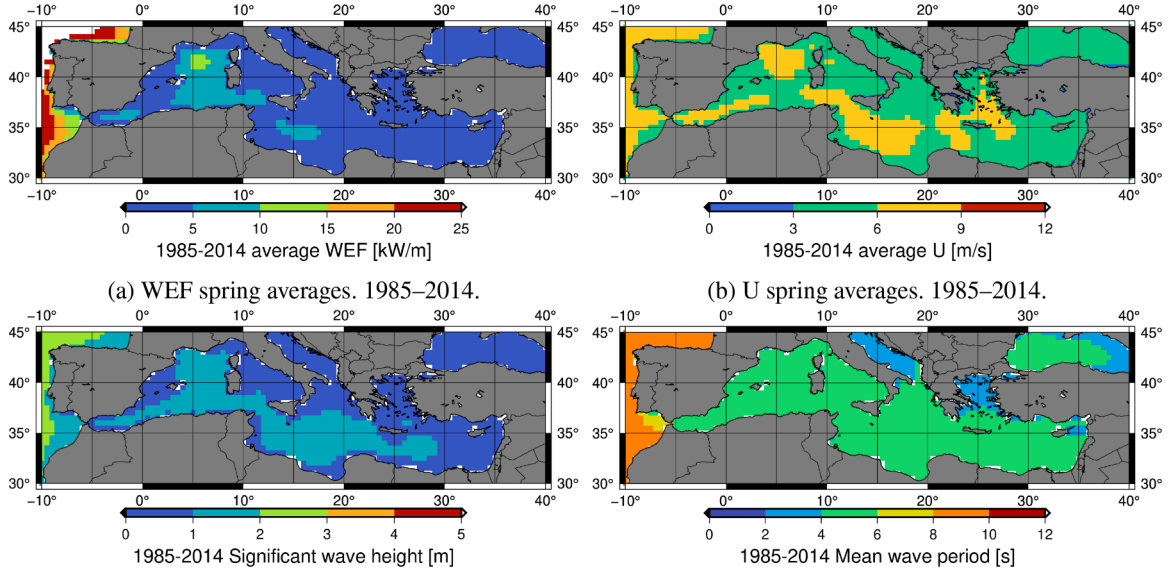

(a) WEF spring averages. 1985–2014.

(b) U spring averages. 1985–2014.

(c) H_s spring averages. 1985–2014.

(d) T_m spring averages. 1985–2014.

Fig. A2. ERA5 spring averages. 1985–2014.

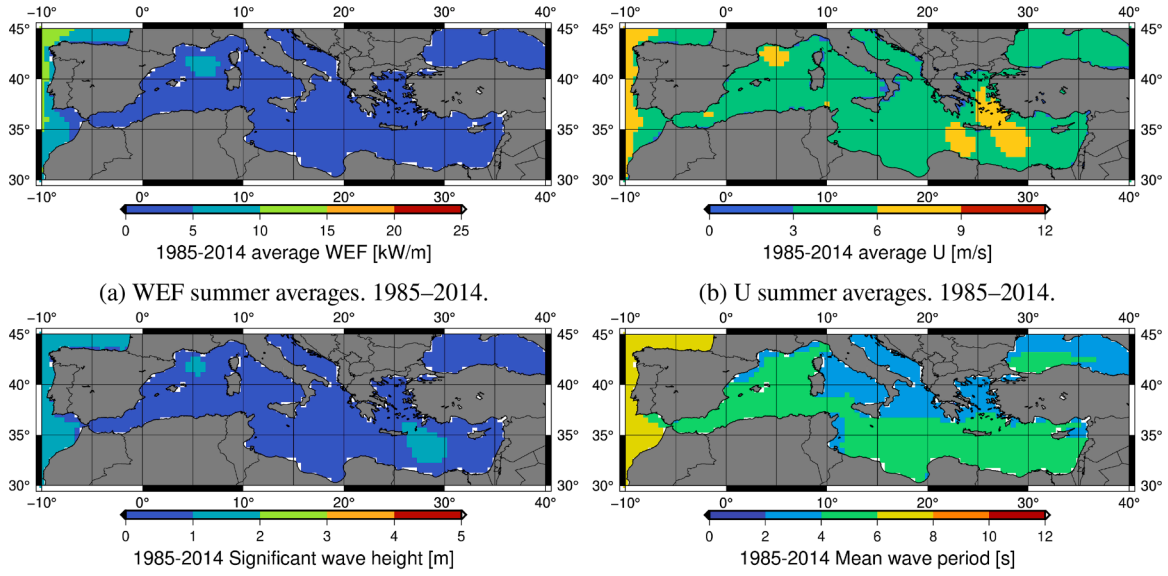

(a) WEF summer averages. 1985–2014.

(b) U summer averages. 1985–2014.

(c) H_s summer averages. 1985–2014.

(d) T_m summer averages. 1985–2014.

Fig. A3. ERA5 summer averages. 1985–2014.

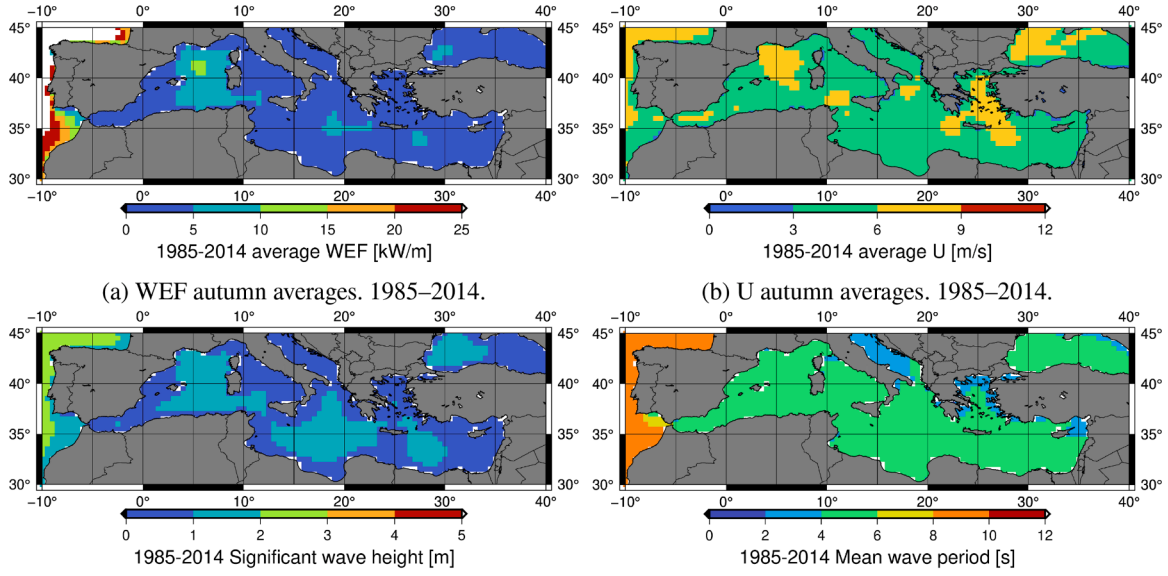

(a) WEF autumn averages. 1985–2014.

(b) U autumn averages. 1985–2014.

(c) H_s autumn averages. 1985–2014.

(d) T_m autumn averages. 1985–2014.

Fig. A4. ERA5 autumn averages. 1985–2014.

Appendix B. Seasonal trends. SSP126

B. 2015–2100 seasonal trends for the four variables and the SSP126 scenario.

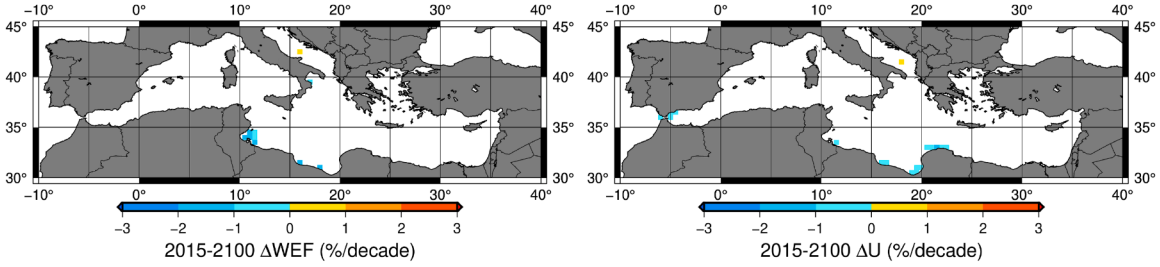

(a) WEF winter seasonal trends. SSP126 scenario (b) U winter seasonal trends. SSP126 scenario

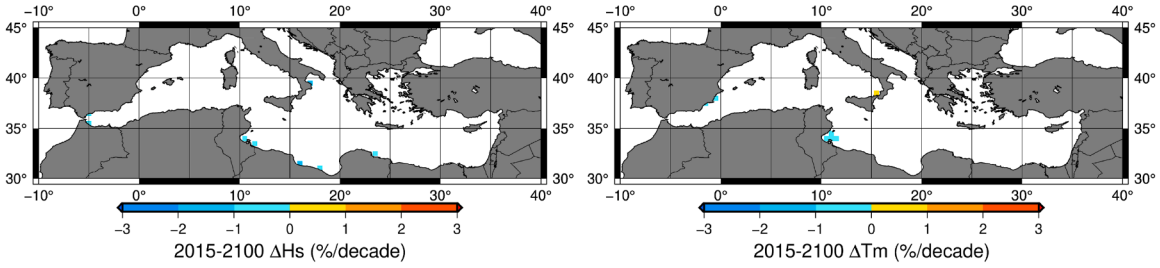

(c) H_s winter seasonal trends. SSP126 scenario (d) T_m winter seasonal trends. SSP126 scenario

Fig. B1. CMIP6-derived 2015–2100 winter seasonal trends [%]/decade with respect to the 1985–2014 period. SSP126 scenario.

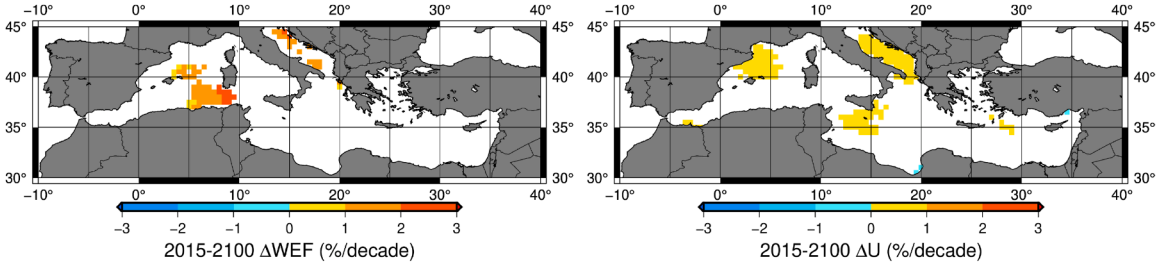

(a) WEF spring seasonal trends. SSP126 scenario (b) U spring seasonal trends. SSP126 scenario

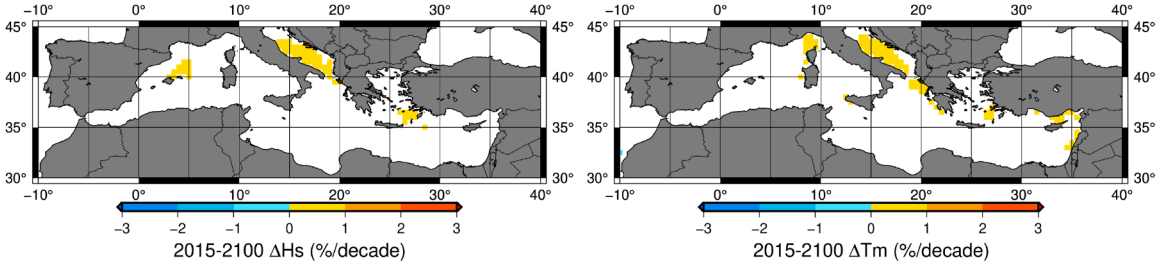

(c) H_s spring seasonal trends. SSP126 scenario (d) T_m spring seasonal trends. SSP126 scenario

Fig. B2. CMIP6-derived 2015–2100 spring seasonal trends [%]/decade with respect to the 1985–2014 period. SSP126 scenario.

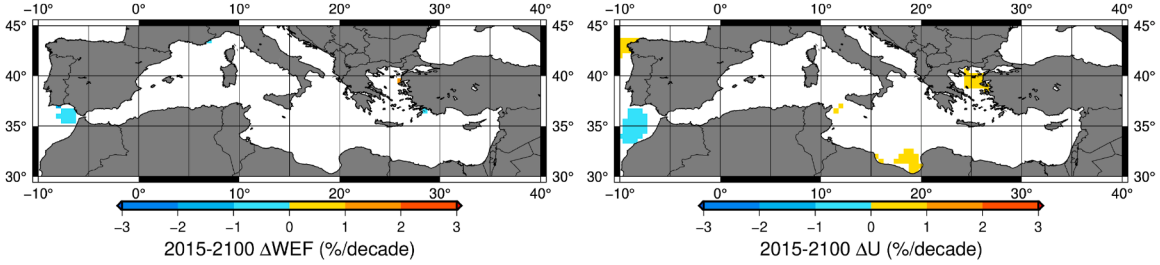

(a) WEF summer seasonal trends. SSP126 scenario (b) U summer seasonal trends. SSP126 scenario

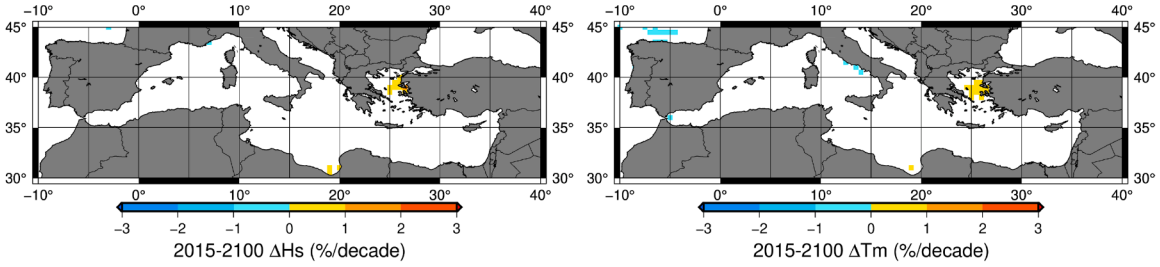

(c) H_s summer seasonal trends. SSP126 scenario (d) T_m summer seasonal trends. SSP126 scenario

Fig. B3. CMIP6-derived 2015–2100 summer seasonal trends [%]/decade with respect to the 1985–2014 period. SSP126 scenario.

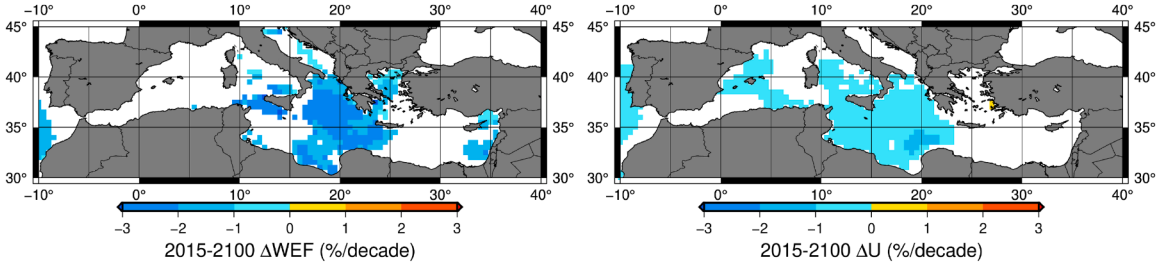

(a) WEF autumn seasonal trends. SSP126 scenario (b) U autumn seasonal trends. SSP126 scenario

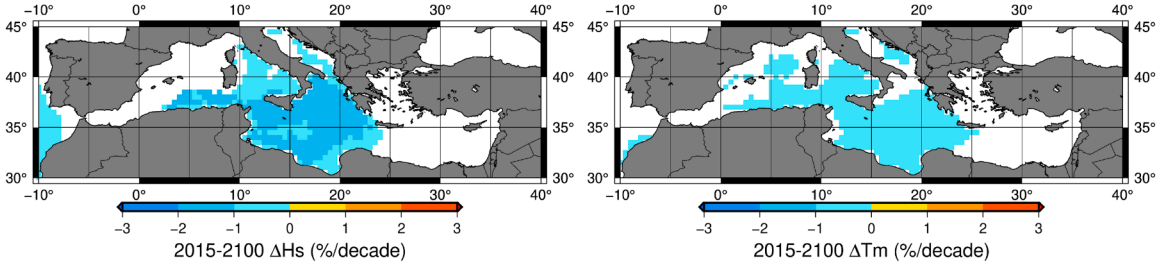

(c) H_s autumn seasonal trends. SSP126 scenario (d) T_m autumn seasonal trends. SSP126 scenario

Fig. B4. CMIP6-derived 2015–2100 autumn seasonal trends [%]/decade with respect to the 1985–2014 period. SSP126 scenario.

Appendix C. Seasonal trends. SSP585

C. 2015–2100 seasonal trends for the four variables and the SSP585 scenario.

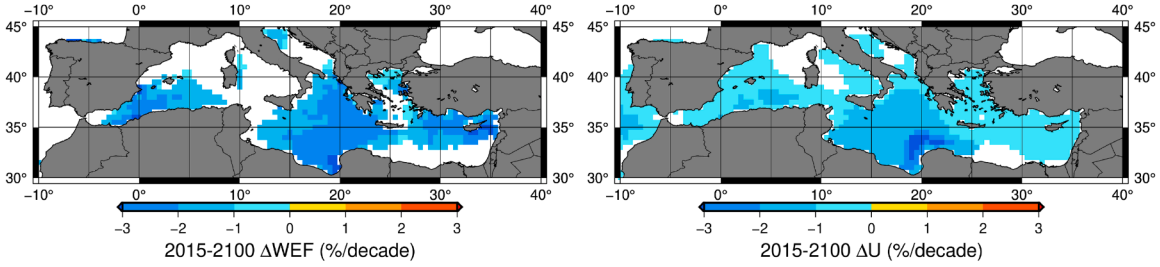

(a) WEF winter seasonal trends. SSP585 scenario (b) U winter seasonal trends. SSP585 scenario

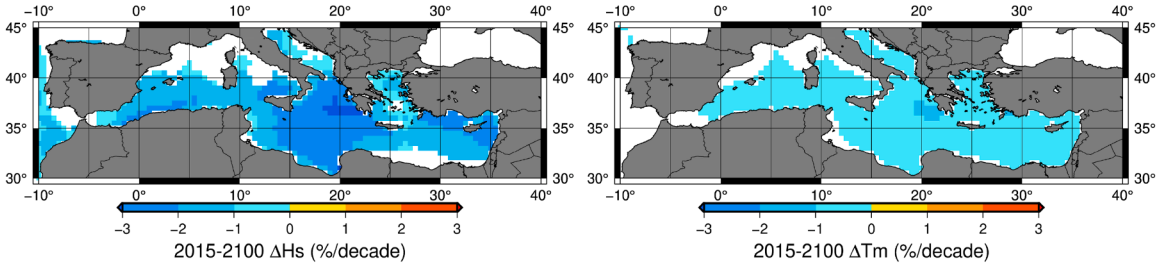

(c) H_s winter seasonal trends. SSP585 scenario (d) T_m winter seasonal trends. SSP585 scenario

Fig. C1. CMIP6-derived 2015–2100 winter seasonal trends [%]/decade with respect to the 1985–2014 period. SSP585 scenario.

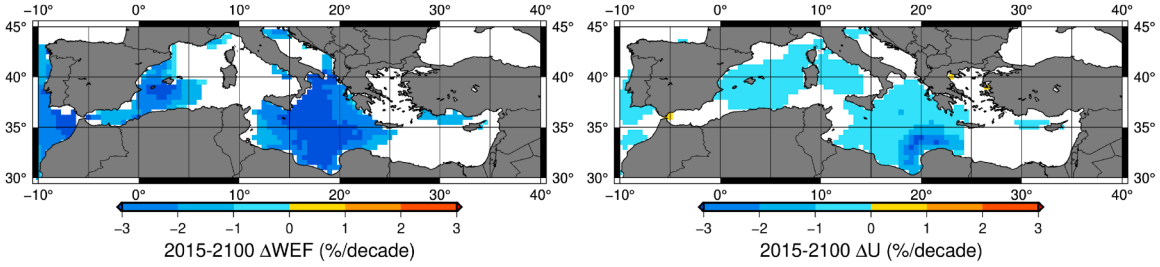

(a) WEF spring seasonal trends. SSP585 scenario (b) U spring seasonal trends. SSP585 scenario

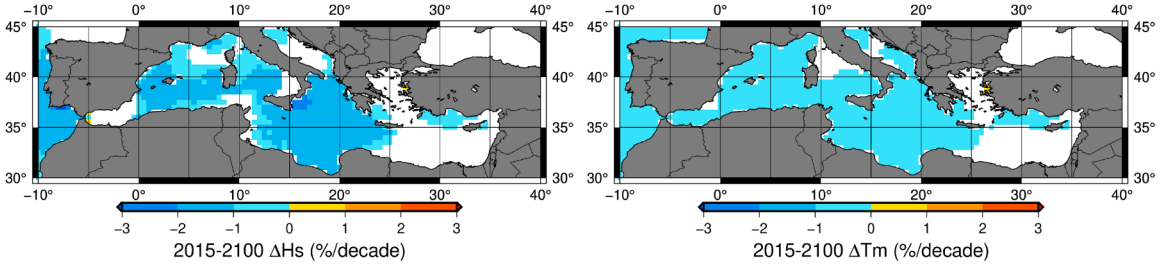

(c) H_s spring seasonal trends. SSP585 scenario (d) T_m spring seasonal trends. SSP585 scenario

Fig. C2. CMIP6-derived 2015–2100 spring seasonal trends [%]/decade with respect to the 1985–2014 period. SSP585 scenario.

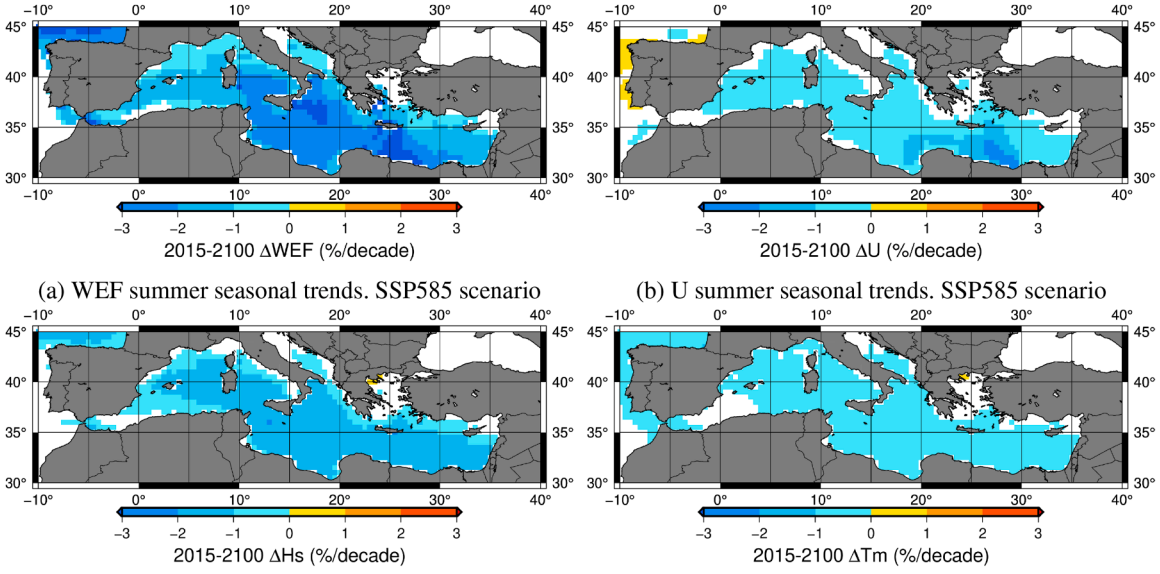

(a) WEF summer seasonal trends. SSP585 scenario

(b) U summer seasonal trends. SSP585 scenario

(c) H_s summer seasonal trends. SSP585 scenario

(d) T_m summer seasonal trends. SSP585 scenario

Fig. C3. CMIP6-derived 2015–2100 summer seasonal trends [%]/decade with respect to the 1985–2014 period. SSP585 scenario.

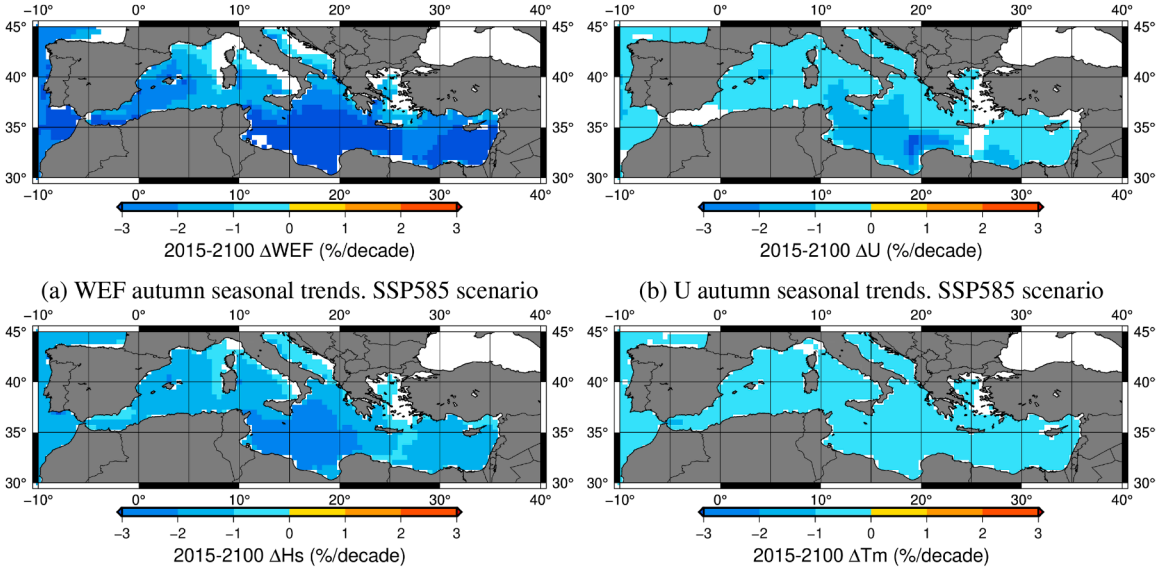

(a) WEF autumn seasonal trends. SSP585 scenario

(b) U autumn seasonal trends. SSP585 scenario

(c) H_s autumn seasonal trends. SSP585 scenario

(d) T_m autumn seasonal trends. SSP585 scenario

Fig. C4. CMIP6-derived 2015–2100 autumn seasonal trends [%]/decade with respect to the 1985–2014 period. SSP585 scenario.

References

American Meteorological Society, 2022. Climatological standard normals, Glossary of Meteorology. https://glossary.ametsoc.org/wiki/Climatological_standard_normals.

Barbariol, F., Davison, S., Falcieri, F.M., Ferretti, R., Ricchi, A., Sclavo, M., Benetazzo, A., 2021. Wind waves in the Mediterranean sea: an ERA5 reanalysis wind-based climatology. Front. Mar. Sci. 8, 760614.

Bi, D., Dix, M., Marsland, S., O'farrell, S., Sullivan, A., Bodman, R., Law, R., Harman, I., Srbinovsky, J., Rashid, H.A., et al., 2020. Configuration and spin-up of ACCESS-CM2, the new generation australian community climate and earth system simulator coupled model. J. Southern Hemisphere Earth Syst. Sci. 70 (1), 225–251.

Bidlot, J.-R., 2016. Ocean wave model output parameters. Reading: European Centre for Medium-Range Weather Forecasts (ECMWF) https://confluence.ecmwf.int/download/attachments/59774192/wave_parameters.pdf.

Cahill, B., Lewis, T., 2014. Wave periods and the calculation of wave power. Proceedings of the 2nd Marine Energy Technology Symposium METS2014 April 15–18, 2014, Seattle, WA.

Camus, P., Herrera, S., Gutiérrez, J.M., Losada, I.J., 2019. Statistical downscaling of seasonal wave forecasts. Ocean Model. 138, 1–12.

Carreno-Madinabeitia, S., Serras, P., Ibarra-Berastegui, G., Sáenz, J., Ulazia, A., 2024. Future electricity production at mutriku wave energy plant estimated from CMIP6 wave climate projections (2015–2100). Ocean Eng. 291, 116624. https://doi.org/10.1016/j.oceaneng.2023.116624

Casas-Prat, M., Wang, X.L., Swart, N., 2018. CMIP5-based global wave climate projections including the entire Arctic ocean. Ocean Model. 123, 66–85.

Clarke, D.C., Richardson, M., 2021. The benefits of continuous local regression for quantifying global warming. Earth Space Sci. 8 (5), e2020EA001082.

De Leo, F., Briganti, R., Besio, G., 2024. Trends in ocean waves climate within the Mediterranean sea: a review. Clim. Dyn. 62 (2), 1555–1566.

DKRZ, 2022. The SSP scenarios. Last accessed: 2024-12-10. https://www.dkrz.de/en/communication/climate-simulations/cmip6-en/the-ssp-scenarios/.

Döscher, R., Acosta, M., Alessandri, A., Anthoni, P., Arneth, A., Arsouze, T., Bergmann, T., Bernadello, R., Bousetta, S., Caron, L.-P., et al., 2021. The EC-earth3 earth system model for the climate model intercomparison project 6. Geosci. Model. Dev. Discuss. 2021, 1–90.

ECMWF, 2021. Changing the reference period from 1981 to 2020 to 1991–2020 for the c3s climate bulletin. https://climate.copernicus.eu/sites/default/files/2021-02/C3S_Climate_Bulletin_change_from_1981-2010_to_1991-2020_reference_period_v08-Feb-20_all.pdf.

ECMWF, 2021. Ifs documentation cy47r3—Part VII: Ecmwf wave model. (09/2021 2021). https://doi.org/10.21957/zz4bj65vr

ECMWF, 2024. Climate Data Store, Copernicus Climate Change Service. https://cds.climate.copernicus.eu/cdsapp#!/home.

Elshinnawy, A.I., Antolínez, J. A., 2023. A changing wave climate in the Mediterranean sea during 58-years using UERRA-MESCAN-SURFEX high-resolution wind fields. Ocean Eng. 271, 113689. https://doi.org/10.1016/j.oceaneng.2023.113689

Erikson, L., Morim, J., Hemer, M., Young, I., Wang, X.L., Mentaschi, L., Mori, N., Semedo, A., Stopa, J., Grigorieva, V., et al., 2022. Global ocean wave fields show consistent regional trends between 1980 and 2014 in a multi-product ensemble. Commun. Earth Environ. 3 (1), 320.

Esnaola, G., Ulazia, A., Sáenz, J., Ibarra-Berastegi, G., 2024. Future changes of global annual and seasonal wind-energy production in CMIP6 projections considering air density variation. Energy 307, 132706.

Ewans, K., Jonathan, P., 2023. Uncertainties in estimating the effect of climate change on 100-year return value for significant wave height. Ocean Eng. 272, 113840.

Gao, H., Liang, B., Shao, Z., 2021. A global climate analysis of wave parameters with a focus on wave period from 1979 to 2018. Appl. Ocean Res. 111, 102652.

Gleisner, H., 2011. GRAS SAF Report 10. Latitudinal Binning and Area-Weighted Averaging of Irregularly Distributed Radio Occultation Data. Technical Report. EUMETSAT.

Hellmuth, F., Carlsen, T., Daloz, A.S., David, R.O., Che, H., Storelvmo, T., 2025. Evaluation of biases in mid-to-high-latitude surface snowfall and cloud phase in ERA5 and CMIP6 using satellite observations. Atmos. Chem. Phys. 25, 1353–1383. https://doi.org/10.5194/acp-25-1353-2025

Hersbach, H., Bell, B., Berrisford, P., Hirahara, S., Horányi, A., Muñoz-Sabater, J., Nicolas, J., Peubey, C., Radu, R., Schepers, D., et al., 2020. The ERA5 global reanalysis. Q. J. R. Meteorolog. Soc. 146 (730), 1999–2049.

Holthuijsen, L.H., Booij, N., Ris, R.C., 2023. SWAN Simulating Waves Nearshore. Last accessed: 2024-12-10. https://swanmodel.sourceforge.io/.

Ibarra-Berastegui, G., Sáenz, J., Ulazia, A., Sáenz-Aguirre, A., Esnaola, G., 2023. CMIP6 projections for global offshore wind and wave energy production (2015–2100). Sci. Rep. 13 (1), 18046. https://doi.org/10.1038/s41598-023-45450-3

IPCC, 2022. (International Panel on Climate Change), Summary for Policy Makers, Climate Change 2022: Impacts, adaptation and vulnerability (2022). Last accessed: 2024-12-10. https://doi.org/{10.1017/9781009325844.001}.

Iturbide, M., Gutiérrez, J.M., Alves, L.M., Bedia, J., Cimadevilla, E., Cofiño, A.S., Cerezo-Mota, R., Di Luca, A., Faria, S.H., Gorodetskaya, I., et al., 2020. An update of IPCC climate reference regions for subcontinental analysis of climate model data: definition and aggregated datasets. Earth Syst. Sci. Data Discuss. 2020, 1–16.

Jiang, X., Xie, B., Bao, Y., Song, Z., 2023. Global 3-hourly wind-wave and swell data for wave climate and wave energy resource research from 1950 to 2100. Sci. Data 10 (1), 225.

Kajtar, J.B., Santoso, A., Collins, M., Taschetto, A.S., England, M.H., Frankcombe, L.M., 2021. Cmip5 intermodel relationships in the baseline southern ocean climate system and with future projections. Earth's Future 9 (6), e2020EF001873.

Kim, D., Song, S., Turnock, S., Tezdogan, T., 2023. Nonlinear URANS model for path-following control problem towards autonomous marine navigation under wave conditions. Ocean Eng. 270, 113681. https://doi.org/10.1016/j.oceaneng.2023.113681

Komsta, L., 2019. mblm: Median-Based Linear Models. R package version 0.12.1. https://CRAN.R-project.org/package=mblm.

Kriegler, E., Edmonds, J., Hallegatte, S., Ebi, K.L., Kram, T., Riahi, K., Winkler, H., Van Vuuren, D.P., 2014. A new scenario framework for climate change research: the concept of shared climate policy assumptions. Clim. Change 122, 401–414.

Kumar, S.P., 1968. Estimates of the regression coefficient based on Kendall's tau. J. Am. Stat. Assoc. 63 (324), 1379–1389.

Lee, H., Romero, J., 2023. Summary for policymakers. in: Climate change 2023: Synthesis report. A report of the intergovernmental panel on climate change. contribution of working groups I, II and III to the sixth assessment report of the intergovernmental panel on climate change. Last accessed: 2024-12-10. https://www.ipcc.ch/report/ar6/syr/.

Lemos, G., Semedo, A., Dobrynin, M., Behrens, A., Staneva, J., Bidlot, J.-R., Miranda, P. M.A., 2019. Mid-twenty-first century global wave climate projections: results from a dynamic CMIP5 based ensemble. Glob. Planet. Change 172, 69–87.

Lionello, P., Giorgi, F., Rohling, E., Seager, R., 2023. Chapter 3—Mediterranean climate: past, present and future. In: Schroeder, K., Chiggiato, J. (Eds.), Oceanography of the Mediterranean Sea. Elsevier, pp. 41–91. https://doi.org/10.1016/B978-0-12-823692-5.00011-X

Lira-Loarca, A., Ferrari, F., Mazzino, A., Besio, G., 2021. Future wind and wave energy resources and exploitability in the Mediterranean Sea by 2100. Appl. Energy 302, 117492.

Liu, J., Meucci, A., Young, I.R., 2023. A comparison of multiple approaches to study the modulation of ocean waves due to climate variability. J. Geophys. Res. 128 (9), e2023JC019843.

Lobeto, H., Menendez, M., Losada, I.J., 2021. Future behavior of wind wave extremes due to climate change. Sci. Rep. 11 (1), 1–12.

Martinez, A., Iglesias, G., 2021. Wind resource evolution in europe under different scenarios of climate change characterised by the novel shared socioeconomic pathways. Energy Convers. Manag. 234, 113961.

Martinez, A., Iglesias, G., 2023. Climate-change impacts on offshore wind resources in the Mediterranean sea. Energy Convers. Manag. 291, 117231.

Masson-Delmotte, V., Zhai, P., Pirani, A., Connors, S.L., Péan, C., Berger, S., Caud, N., Chen, Y., Goldfarb, L., Gomis, M.I., et al., 2021. Climate change 2021: the physical science basis. Contribution of Working Group I to the Sixth Assessment Report of the Intergovernmental Panel on Climate Change 2.

Meehl, G.A., Senior, C.A., Eyring, V., Flato, G., Lamarque, J.-F., Stouffer, R.J., Taylor, K.E., Schlund, M., 2020. Context for interpreting equilibrium climate sensitivity and transient climate response from the CMIP6 earth system models. Sci. Adv. 6, 1981. https://doi.org/10.1126/sciadv.aba1981

Meucci, A., Young, I., Hemer, M., Trenham, C., 2021a. CMIP6 global wind-wave 21st century climate projections - combined CSIRO. Service collection. Data, https://data.csiro.au/collection/csiro:60106.

Meucci, A., Young, I., Hemer, M., Trenham, C., 2021b. CMIP6 global wind-wave 21st century climate projections phase 1. v6. CSIRO. Service collection. Data. http://hdl.handle.net/102.100.100/432508?index=1.

Meucci, A., Young, I.R., Hemer, M., Trenham, C., Watterson, I.G., 2023. 140 years of global ocean wind-wave climate derived from CMIP6 ACCESS-CM2 and EC-Earth3 GCMs: Global trends, regional changes, and future projections. J. Clim., 36 (6), 1605–1631.

Meucci, A., Young, I.R., Trenham, C., Hemer, M., 2024. An 8-model ensemble of CMIP6-derived ocean surface wave climate. Sci. Data 11 (1), 100.

Mori, N., Shimura, T., Yasuda, T., Mase, H., 2013. Multi-model climate projections of ocean surface variables under different climate scenarios–future change of waves, sea level and wind. Ocean Eng. 71, 122–129.

Morim, J., Trenham, C., Hemer, M., Wang, X.L., Mori, N., Casas-Prat, M., Semedo, A., Shimura, T., Timmermans, B., Camus, P., et al., 2020. A global ensemble of ocean wave climate projections from CMIP5-driven models. Sci. Data 7 (1), 1–10.

Multon, B., 2013. Marine Renewable Energy Handbook. John Wiley and Sons.

North, G.R., Bell, T.L., Cahalan, R.F., Moeng, F.J., 1982. Sampling errors in the estimation of empirical orthogonal functions. Mon. Weather Rev. 110 (7), 699–706. https://doi.org/10.1175/1520-0493(1982)110<0699:SEITEO>2.0.CO;2

Odériz, I., Mori, N., Shimura, T., Webb, A., Silva, R., Mortlock, T.R., 2022. Transitional wave climate regions on continental and polar coasts in a warming world. Nat. Clim. Change 12 (7), 662–671.

Odériz, I., Silva, R., Mortlock, T.R., Mori, N., 2020. El niño-southern oscillation impacts on global wave climate and potential coastal hazards. J. Geophys. Res. 125 (12), e2020JC016464.

Odériz, I., Silva, R., Mortlock, T.R., Mori, N., Shimura, T., Webb, A., Padilla-Hernández, R., Villers, S., 2021. Natural variability and warming signals in global ocean wave climates. Geophys. Res. Lett. 48 (11), e2021GL093622.

O'Neill, B.C., Tebaldi, C., Van Vuuren, D.P., Eyring, V., Friedlingstein, P., Hurtt, G., Knutti, R., Kriegler, E., Lamarque, J.-F., Lowe, J., et al., 2016. The scenario model intercomparison project (scenarioMIP) for CMIP6. Geosci. Model Dev. 9 (9), 3461–3482.

Patra, A., Min, S.-K., Kumar, P., Wang, X.L., 2021a. Changes in extreme ocean wave heights under 1.5°C, 2°C, and 3°C global warming. Weather Clim. Extremes 33, 100358.

Patra, A., Min, S.-K., Son, S.-W., Yeh, S.-W., 2021b. Hemispheric asymmetry in future wave power changes: seasonality and physical mechanisms. J. Geophys. Res. 126 (12), e2021JC017687.

Penalba, M., Ulazia, A., Saénz, J., Ringwood, J.V., 2020. Impact of long-term resource variations on wave energy farms: the icelandic case. Energy 192, 116609.

Pourali, M., Kavianpour, M.R., Kamranzad, B., Alizadeh, M.J., 2023. Future variability of wave energy in the Gulf of Oman using a high resolution CMIP6 climate model. Energy 262, 125552.

Power, E., 2024. Israeli Firm Launches Middle East's First Grid-Connected Wave Energy Plant. Last accessed: 2024-12-10. Israeli Firm Launches Middle East's First Grid-Connected Wave Energy Plant.

Ramos, M.S., Farina, L., Faria, S.H., Li, C., 2021. Relationships between large-scale climate modes and the South Atlantic Ocean wave climate. Prog. Oceanogr. 197, 102660.

R Core Team, 2023. R: A Language and Environment for Statistical Computing. R Foundation for Statistical Computing. Vienna, Austria. https://www.R-project.org/.

Reguero, B.G., Losada, I.J., Méndez, F.J., 2015. A global wave power resource and its seasonal, interannual and long-term variability. Appl. Energy 148, 366–380.

Reguero, B.G., Losada, I.J., Méndez, F.J., 2019. A recent increase in global wave power as a consequence of oceanic warming. Nat. Commun. 10 (1), 1–14. https://doi.org/10.1038/s41467-018-08066-0

Riahi, K., Van Vuuren, D.P., Kriegler, E., Edmonds, J., O'neill, B.C., Fujimori, S., Bauer, N., Calvin, K., Dellink, R., Fricko, O., et al., 2017. The shared socioeconomic pathways and their energy, land use, and greenhouse gas emissions implications: an overview. Global Environ. Change 42, 153–168.

Rusu, L., 2024. An analysis of the expected wave conditions in the Mediterranean sea in the context of global warming. Ocean Eng. 301, 117487.

Rusu, L., 2025. Climate change impact on the sea state conditions in the Mediterranean sea under RCP and SSP emission scenarios. Renew. Energy 243, 122616. https://doi.org/10.1016/j.renene.2025.122616

Saenz-Aguirre, A., Saenz, J., Ulazia, A., Ibarra-Berastegui, G., 2022a. Optimal strategies of deployment of far offshore co-located wind-wave energy farms. Energy Convers. Manag. 251, 114914.

Saenz-Aguirre, A., Ulazia, A., Ibarra-Berastegi, G., Saenz, J., 2022b. Floating wind turbine energy and fatigue loads estimation according to climate period scaled wind and waves. Energy Convers. Manag. 271, 116303.

Semedo, A., Weisse, R., Behrens, A., Sterl, A., Bengtsson, L., Günther, H., 2012. Projection of global wave climate change toward the end of the twenty-first century. J. Clim. 26 (21), 8269–8288.

Spiridonov, V., Somot, S., Déqué, M., 2023. CNMR Aladin. Last accessed: 2024-12-10. https://www.umr-cnrm.fr/spip.php?article125&langen.

Theil, H., 1950. A rank-invariant method of linear and polynomial regression analysis. Indagationes Mathematicae 12 (85), 173.

Ulazia, A., Ezpeleta, H., Ibarra-Berastegi, G., Sáenz, J., Martinez-Iturricastillo, N., Ringwood, J.V., 2024. Historical trends of floating wind turbine fatigue loads (ireland 1920–2010). Ocean Eng. 299, 117424.

Ulazia, A., Penalba, M., Ibarra-Berastegui, G., Ringwood, J., Saénz, J., 2017. Wave energy trends over the bay of biscay and the consequences for wave energy converters. Energy 141, 624–634.

Ulazia, A., Sáenz, J., Saenz-Aguirre, A., Ibarra-Berastegui, G., Carreno-Madinabeitia, S., 2023a. Paradigmatic case of long-term colocated wind–wave energy index trend in canary islands. Energy Convers. Manag. 283, 116890.

Ulazia, A., Saenz-Aguirre, A., Ibarra-Berastegui, G., Sáenz, J., Carreno-Madinabeitia, S., Esnaola, G., 2023. Performance variations of wave energy converters due to global long-term wave period change (1900–2010). Energy. 268, 126632.

Van Vuuren, D.P., Edmonds, J., Kainuma, M., Riahi, K., Thomson, A., Hibbard, K., Hurtt, G.C., Kram, T., Krey, V., Lamarque, J.-F., et al., 2011. The representative concentration pathways: an overview. Clim. Change 109, 5–31.

Van Vuuren, D.P., Kriegler, E., O'Neill, B.C., Ebi, K.L., Riahi, K., Carter, T.R., Edmonds, J., Hallegatte, S., Kram, T., Mathur, R., et al., 2014. A new scenario framework for climate change research: scenario matrix architecture. Clim. Change 122, 373–386.

Vanem, E., 2017. A regional extreme value analysis of ocean waves in a changing climate. Ocean Eng. 144, 277–295.

Wavewatch III Development Group, 2016. User manual and system documentation of WAVEWATCH III version 5.16. NOAA/NWS/NCEP/MMAB Technical Note 329, 1–326 https://polar.ncep.noaa.gov/waves/wavewatch/manual.v5.16.pdf.

Wessel, P., Luis, J.F., Uieda, L., Scharroo, R., Wobbe, F., Smith, W. H.F., Tian, D., 2019. The generic mapping tools version 6. Geochem., Geophys., Geosyst. 20 (11), 5556–5564. Available at Last accessed: 2024-12-10, https://doi.org/10.1029/2019GC008515

World Climate Research Program, 2021. CMIP6 models repository. Last accessed: 2024-12-10. https://esgf-node.llnl.gov/projects/cmip6/.

World Meteorological Organization, 2017. WMO Guidelines on the Calculation of Climate Normals. Technical Report WMO-No. 1203. WMO. Geneva, Switzerland.

Young, I.R., Ribal, A., 2019. Multiplatform evaluation of global trends in wind speed and wave height. Science 364 (6440), 548–552.